

## Modal analysis for density and anisotropic elasticity identification of adsorbates on microcantilevers

Belardinelli, P.; Hauzer, L. M.F.R.; Šiškins, M.; Ghatkesar, M. K.; Alijani, F.

**DOI**

[10.1063/1.5047279](https://doi.org/10.1063/1.5047279)

**Publication date**

2018

**Document Version**

Accepted author manuscript

**Published in**

Applied Physics Letters

**Citation (APA)**

Belardinelli, P., Hauzer, L. M. F. R., Šiškins, M., Ghatkesar, M. K., & Alijani, F. (2018). Modal analysis for density and anisotropic elasticity identification of adsorbates on microcantilevers. *Applied Physics Letters*, 113(14), Article 143102. <https://doi.org/10.1063/1.5047279>

**Important note**

To cite this publication, please use the final published version (if applicable). Please check the document version above.

**Copyright**

Other than for strictly personal use, it is not permitted to download, forward or distribute the text or part of it, without the consent of the author(s) and/or copyright holder(s), unless the work is under an open content license such as Creative Commons.

**Takedown policy**

Please contact us and provide details if you believe this document breaches copyrights. We will remove access to the work immediately and investigate your claim.

**Modal analysis for density and anisotropic elasticity identification of adsorbates on microcantilevers**

P. Belardinelli,<sup>1</sup> L. M. F. R. Hauzer,<sup>1</sup> M. Šiškins,<sup>2</sup> M. K. Ghatkesar,<sup>1, a)</sup> and F. Alijani<sup>1, b)</sup>

<sup>1)</sup>*Department of Precision and Microsystems Engineering, TU Delft, Mekelweg 2, 2628 CD, Delft, The Netherlands*

<sup>2)</sup>*Kavli Institute of Nanoscience, Quantum Nanoscience Department, TU Delft, Lorentzweg 1, 2628 CJ, Delft, The Netherlands*

(Dated: 15 September 2018)

Physical characteristics like mass and stiffness of biological objects are emerging as new markers for severe diseases. Micromechanical resonators can be used to quantify multiple of these characteristics simultaneously. In this paper, we propose a methodology that utilizes higher flexural modes of vibration to perform simultaneous characterization of density and elastic modulus of adsorbates. To demonstrate this concept, a polymeric block with known dimension and anisotropy is written directly on the cantilever surface using two-photon polymerization technique and characterised by modal analysis. Our method captures the effective bending stress exerted by non-isotropic materials that is masked in atomic force microscopy indentation technique.

PACS numbers: 02.60.Cb, 62.25.Jk

Keywords: Modal analysis, mass and stiffness detection, micromechanical resonators, anisotropic polymerization, **two-photon polymerization, 3D printing polymer**

<sup>a)</sup>Electronic mail: m.k.ghatkesar@tudelft.nl

<sup>b)</sup>Electronic mail: f.aliyani@tudelft.nl

Over the last decades, the development of microsystem technologies has enabled systems that can interact with matter at the micro and nano scale. In this context, nano/micromechanical devices have been proved to be suitable for characterizing mechanical properties of biological systems leading to new insights. Atomic Force Microscopy (AFM) probe was used to distinguish the stiffness of cancer cells from healthy cells<sup>1-3</sup>. Force spectroscopy mode of AFM was used to identify that cancer cells are more elastic than normal cells, which could be the reason for their metastasis. However, biological objects exhibit anisotropic stiffness<sup>4,5</sup> that cannot be measured with force spectroscopy. Similarly, by attaching single cells to the AFM cantilever free-end and continuously monitoring the pico-gram mass changes, mass regulation in different cell states was revealed<sup>6</sup>.

It has been shown that by adsorbing soft objects like bacteria, spread over a small distribution ( $\sim 20\%$ ) on the cantilever surface, either mass or stiffness of the soft objects can be accurately determined<sup>7</sup>. Adsorbing at free-end gave reliable mass measurement and adsorbing at fixed-end gave reliable stiffness. However, by adsorbing at other locations, both mass and stiffness were effected simultaneously<sup>8,9</sup>. The added mass decreases the fundamental resonant frequency whereas the added stiffness increases it<sup>10,11</sup>. Thus, both parameters exhibit counteracting effect on the resonant frequency. In fact, it has been shown that if the effect of stiffness is neglected, mass is underestimated<sup>4</sup>. Therefore, methods to disentangle mass and stiffness for correct quantitative estimations of both are needed<sup>12</sup>.

Gil-Santos et al. used two orthogonal modes of vibration of a nanowire for estimating mass and stiffness of electron-beam-induced carbon deposition<sup>13</sup>. Additional information for the simultaneous resolution of mass, rigidity, and nanoscale heterogeneity of adsorbate has been also provided by estimating damping due to surrounding medium of the cantilever<sup>14</sup>. The mass mechanism governs the resonant frequency response in regions of cantilever resonators with larger vibration amplitude. The stiffness contribution arises for the material adsorbed on nodes almost cancelling the mass effect<sup>8</sup>. Moreover, it was shown that by simultaneous measurement of the first three natural frequencies of a cantilever it is possible to obtain information about mass, stiffness and direction of an adsorbed bacteria<sup>4</sup>.

In this paper, we show that density and anisotropic elasticity of a material shall be disentangled by careful combination of different vibrational modes in multi-modal analysis. Unlike previous reports, we illustrate that focusing only on the first three vibration modes will give erroneous mass measurement results. We also show that the adsorption of material

near fixed-end of the cantilever would suffice to quantify both mass and stiffness properties.

In our experiments, we have deposited a polymer film near the fixed-end of cantilever. A two-photon polymerization technique was used to directly write a polymer layer of desired dimensions<sup>15–17</sup>. Figure 1 shows Scanning Electron Microscope (SEM) images of the two microcantilevers (AFM CONTR type probe from Nano World A.G.) that were used as resonating sensors in our work. Figure 1(a) shows the top view of the first specimen whereas Fig. 1(b) illustrates the lateral view of the second sample. By controlling the writing direction of the laser with respect to the speed and power of the polymerization, an anisotropic adsorbate can intentionally be fabricated<sup>18–20</sup>.

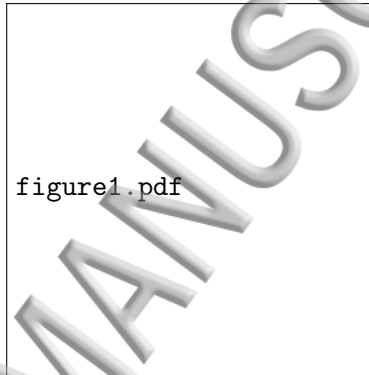


FIG. 1: SEM images of the microcantilever after the deposition of the polymeric block. a) Top view of the first sample, the specimen has length, width and thickness  $\{L_a, W_a, T_a\} = \{45.79, 45.20, 3.28\} \mu\text{m}$ . The cantilever is  $455.21 \mu\text{m}$  long,  $47.13 \mu\text{m}$  wide,  $2 \mu\text{m}$  thick,  $0.12 \text{ N/m}$  stiff with fundamental resonance frequency of  $11.04 \text{ kHz}$ . b) Lateral view of a second sample with dimensions  $\{L_a, W_a, T_a\} = \{47.38, 47, 23, 2.89\} \mu\text{m}$ . The cantilever is  $433.37 \mu\text{m}$  long,  $45.78 \mu\text{m}$  wide,  $2.22 \mu\text{m}$  thick,  $0.17 \text{ N/m}$  stiff with fundamental resonance frequency of  $13.34 \text{ kHz}$ . The added material is highlighted in yellow.

The presence of polymer on top of cantilever changes the dynamic response of the resonator. Figure 2(a) shows the frequency spectra before (in orange) and after (in blue) the polymer addition.

The positive and negative shifts of the resonance frequencies can be directly assessed by accounting for the dual contribution of the added mass and the added stiffness on the cantilever. In order to obtain the natural frequencies of the cantilever in presence of the

polymer adsorbate, Rayleigh-Ritz method has been used<sup>8</sup>:

$$\omega_n^2 = \frac{\int_0^{L_c} D(x) \left( \frac{\partial^2 \psi_n(x)}{\partial x^2} \right)^2 dx}{\int_0^{L_c} (\rho_c W_c T_c + \rho_a W_a T_a(x)) \psi_n^2(x) dx}, \quad (1)$$

in which  $L_c$ ,  $W_c$  and  $T_c$  are the length, width and thickness of the cantilever resonator with density  $\rho_c$ . Moreover,  $T_a$  and  $\rho_a$  are the thickness and density of the added material. With  $\psi_n(x)$  we refer to the flexural vibration mode shapes of the bare cantilever<sup>21</sup> that represent an admissible set of eigenmodes used for the modal decomposition in the linear approximation<sup>7,8,22</sup>. The adsorption on the cantilever does not significantly modify the vibration shapes of the cantilever as experimentally validated comparing the mode shapes of vibration of the bare cantilever and those in the presence of the adsorbate.



FIG. 2: a) Average spectrum of the cantilever beam before (orange) and after (blue) the deposition. The insets are magnification of the frequency shift around the first five flexural modes of the bare cantilever at:  $f_1 = 11.046$  kHz ( $\Delta f_1 = +1.003$  kHz),  $f_2 = 70.893$  kHz ( $\Delta f_2 = +4.194$  kHz),  $f_3 = 199.502$  kHz ( $\Delta f_3 = +7.700$  kHz),  $f_4 = 391.770$  kHz ( $\Delta f_4 = +7.487$  kHz),  $f_5 = 694.359$  kHz ( $\Delta f_5 = -2.304$  kHz). b) Theoretical estimation of the expected frequency shift in presence of the added material ( $E_a = 1.36$  GPa,  $\rho_a = 0.746$  g/cm<sup>3</sup>) for the first five flexural modes as a function of the adsorbate position. The longitudinal axis is the position of the center of mass of the block. The dotted line is the position of the center of mass of the first specimen (Fig. 1(a)).

Due to non-uniform distribution of the sample along the cantilever length,  $T_a = T_a(x)$ . Finally,  $E_c$  and  $E_a$  are the Young's modulus of the cantilever and the added material,

respectively. The bending rigidity  $D(x)$  of the cantilever-adsorbate system is a function of the longitudinal spatial coordinate ( $x$ ) and it accounts for the neutral axis shift due to the adsorbate layer<sup>23</sup>. In the absence of added material, this stiffness measure reduces to the product of the modulus of elasticity  $E_c$  and the moment of inertia  $W_c T_c^3/12$ . The model assumes that the adsorbate longitudinal dimension is much larger than the thickness and thus the adsorbate can effectively be regarded as a thin layer deposited on the cantilever<sup>22</sup>. The case of single biological entities, e.g. proteins and viruses, has to be differently tackled accounting for the deformation during the adsorption process due to interfacial energy, adsorption direction and low bending rigidity<sup>5</sup>.

Figure 2(b) shows the expected frequency shift induced by the adsorption of the material at different locations of the resonator, numerically. It can be observed that the deposition close to the clamped edge (dotted line) results in a positive shift in the first four flexural frequencies, while the frequency shift is negative for the fifth mode of vibration, confirming the trend observed in Fig. 2(a).

In order to identify density and Young's modulus simultaneously, we minimize the weighted difference of experimentally obtained resonance frequencies and those obtained using equation (1) keeping  $\rho_a$  and  $E_a$  as the free parameters. Our minimization approach accounts for the first resonance frequency (mode  $i$ ) combined with a higher mode of vibration (mode  $j$ )<sup>24</sup>, in terms of relative shifts, as shown in equation (2). The error is then minimized to obtain  $E_a$  and  $\rho_a$ .

$$\text{err}_{\text{RMS}}(E_a, \rho_a) = \sqrt{\frac{1}{2} \left[ \left( \frac{\omega_i - \omega_i^{\text{exp}}}{\omega_i} \right)^2 + \left( \frac{\omega_j - \omega_j^{\text{exp}}}{\omega_j} \right)^2 \right]} \quad (2)$$

The result is reported in Table I. The accuracy of the identification technique increases by exploiting higher flexural modes as a result of a larger mass contribution. Since the polymer is located at the clamped edge of the resonator, the first mode provides information on the stiffness but is not able to realize the mass effect. It can be observed that, unlike the common belief of utilizing the first two resonance frequencies for obtaining information on both mass and stiffness, using the first two modes in this case can lead to unrealistic values. The use of the first and the fifth frequency, bounds the total error on the five flexural frequencies to less than 4.23%.

Combination of modes	$E_a$ (GPa)	$\rho_a$ (g/cm <sup>3</sup> )
1 <sup>st</sup> flex. mode + 2 <sup>nd</sup> flex. mode	1.44	-65.77
1 <sup>st</sup> flex. mode + 3 <sup>rd</sup> flex. mode	1.40	-0.96
1 <sup>st</sup> flex. mode + 4 <sup>th</sup> flex. mode	1.39	-1.62
1 <sup>st</sup> flex. mode + 5 <sup>th</sup> flex. mode	1.36	0.74

TABLE I: Identified values for the elasticity ( $E_a$ ) and density ( $\rho_a$ ) of the added polymer with different combinations of flexural modes (equation (2)).

To investigate the suitability of modal analysis for capturing the anisotropic nature of adsorbates, a second experiment is then performed with an orthogonal writing direction (i.e. laser direction for polymerization was along  $y$  axis). The estimation based on the frequency shift lead to an elasticity significantly less than the previous case  $E_a = 0.41$  GPa and  $\rho_a = 0.53$  g/cm<sup>3</sup>.

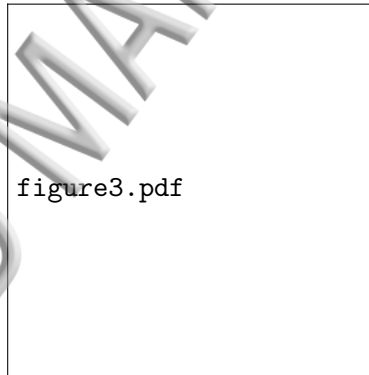


FIG. 3: Identification of the mechanical properties considering an uncertainty of 5% in the three dimensions of the deposited material. a) Distribution for the specimens elasticity  $E_a$ .

In the insets, we show the different specimens with their writing directions under deformation. b) Distribution for the specimens density  $\rho_a$ .

The identification procedure is extended by accounting for small geometric imperfections and the multiple detection process is repeated by varying the polymeric block dimensions. The distribution of obtained values for both Young's modulus and density is reported in Fig. 3.

The distributions, in which the density is detected, present an overlapping region around

0.55 g/cm<sup>3</sup> (see Fig. 3(b)). The two-photon polymerization technique can lead to a small variability in the density of the polymerized material. This is particularly delicate in the case of changing the printing direction that can induce different overlaps of the three dimensional voxels of the two-photon polymerized material. Since the laser intensity defines the material structure locally, the photoresist is excited each time in a different way, and only when a specific volume in the focus point of the laser has enough energy to overcome the polymerization threshold, the material is effectively printed. The length and diameter of an oval shaped voxel in the two-photon polymerized process is a very sensitive parameter of exposure time. Furthermore, the overlap error due to geometrical errors in stage motion during printing and errors due to translation of CAD models to print cannot be ignored. Thus, the variability on the density is associated with the single local voxel properties induced by the fabrication process. The histograms relative to the sample elasticity are instead highly dissimilar as can be seen from Fig. 3(a). This difference is related to the different polymerisation directions of the polymeric block on the cantilever surface. The insets of Fig. 3(a) provide a qualitative scenario of the deformation of the polymeric structure subjected to the bending moment caused by the cantilever's flexural modes of vibration.

To better understand the difference between responses of the two specimens, a further investigation was performed by an AFM force spectroscopy in contact regime (Bruker AFM). The measures of the elasticity were obtained by force spectroscopy technique. Figure 4(a) shows the topography of the polymeric block obtained by AFM. It can be observed that the polymerisation direction for this polymer block was along the longitudinal axis of the beam. Indentation of the material provides the data to estimate the Young's modulus of the polymer (circles in Fig. 4(b)). The Hertz model,  $F = \frac{4}{3} \frac{E_a}{(1 - \nu_a)} \sqrt{r} \delta^{\frac{3}{2}}$  ( $F$  being the force exerted on the polymer and  $\delta$  the induced indentation) has been used to fit the experimental data yielding a Young's modulus of  $1.42 \pm 0.32$  GPa in good agreement with the one estimated by the modal analysis. The knowledge of the tip radius is essential for estimating the Young's modulus with accuracy and this can be quantified either ex-situ by using SEM or in-situ using a dynamical method<sup>25</sup>. In this work the tip radius was measured by SEM and was found to be  $r = 7 \pm 2$ . The estimated value and error is due to the normal distribution fit at fixed  $r = 7$  nm radius. Moreover, in calculating the fits Poisson's ratio was assumed to be  $\nu_a = 0.33$  from literature for fast contact with viscoelastic material<sup>26-28</sup>.

The AFM image of the second sample shown in Fig. 4(c) highlights the material direction

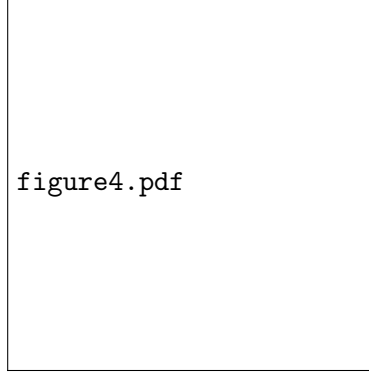


FIG. 4: a) Topography image of the first polymeric sample block ( $x$  is the longitudinal axis along the cantilever length,  $y$  the dimension in the cantilever width axis). b) Estimation of the Young's modulus with AFM indentation technique (force spectroscopy). The red curve is the fit of the Hertz model to the experimental data ( $\circ$ ). In the inset, the histogram of several indentations is shown. Each count is an average of 3 to 5 indentations at the same point. c) Topography image of the second polymeric sample block ( $x$  is the longitudinal axis along the cantilever length,  $y$  the dimension in the cantilever width axis). d) Estimation of the Young's modulus with AFM indentation technique (force spectroscopy). The red curve is the fit of Hertz model to the experimental data ( $\circ$ ). In the inset the histogram of several indentations is given and each count is an average of 3 to 5 indentations at the same point.

along the  $y$  axis. Here, the AFM indentation provides values similar to the previous experiment (Fig. 4(d)) since the material is still locally isotropic and the AFM is not capable of capturing the global response of the material under the effect of an induced deformation. Indeed, it is the global effect of the distribution of the structure that creates the bending

Sample	Measure	$E_a$ (GPa)	$\rho_a$ (g/cm <sup>3</sup> )
1	AFM	$1.42 \pm 0.32$	/
	MA	$1.36 \pm 0.24$	$0.75 \pm 0.32$
2	AFM	$1.75 \pm 0.36$	/
	MA	$0.45 \pm 0.11$	$0.47 \pm 0.17$

TABLE II: Summary of the identified properties by making use of AFM and modal analysis (MA) method.

stiffness of the additional layer. Thus, the orthogonal alignment of the fibres with respect to the elongation/constriction axis, limits the opposition to the deformation during both stretching and compression, i.e. it reduces the effective stiffness. Conversely, the polymer presented in Fig. 4(a) acts homogeneously in the direction of the deformation ( $x$ ). Table II summarizes the attained material properties using both modal analysis and AFM.

In summary we have shown that: i) the deconvolution of mass and effective Young's modulus of the adsorbate is highly sensitive to the utilization of the correct combination of flexural modes of vibration. Indeed, for a deposition location at the fixed-end, higher flexural modes play an important role on determining the accuracy of the extracted properties; ii) our proposed methodology does not require amplitude calibration as it only considers the extracted frequencies; iii) unlike other approaches, adsorption of the material under investigation near the fixed-end would suffice to extract density, elasticity and anisotropic information.

To conclude, our results show that the correct choice and combination of higher flexural modes with fundamental mode is necessary for evaluation of density, elasticity and anisotropy of the adsorbed material on the cantilever. We believe this research could trigger a development of more sophisticated methods for studies of complex mechanical characteristics of various biological samples.

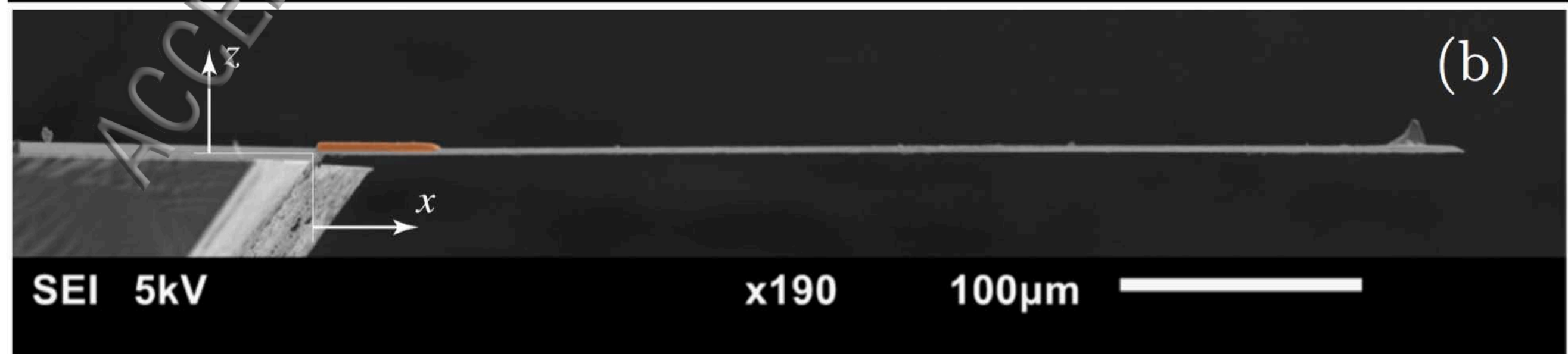
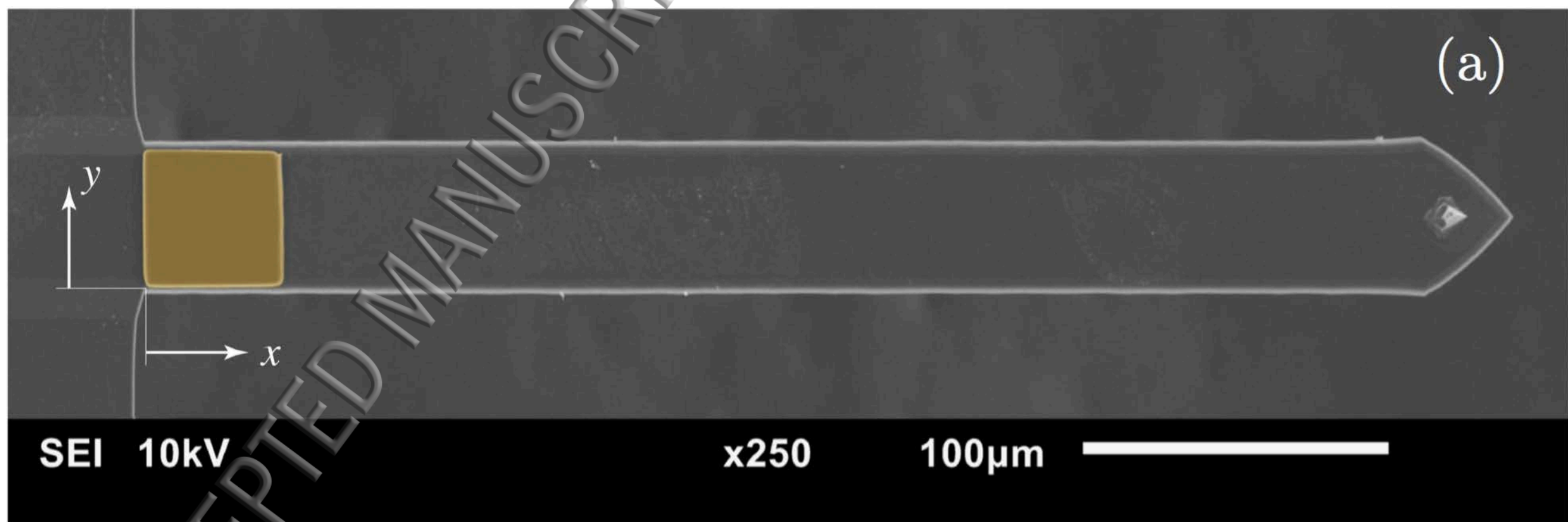
## REFERENCES

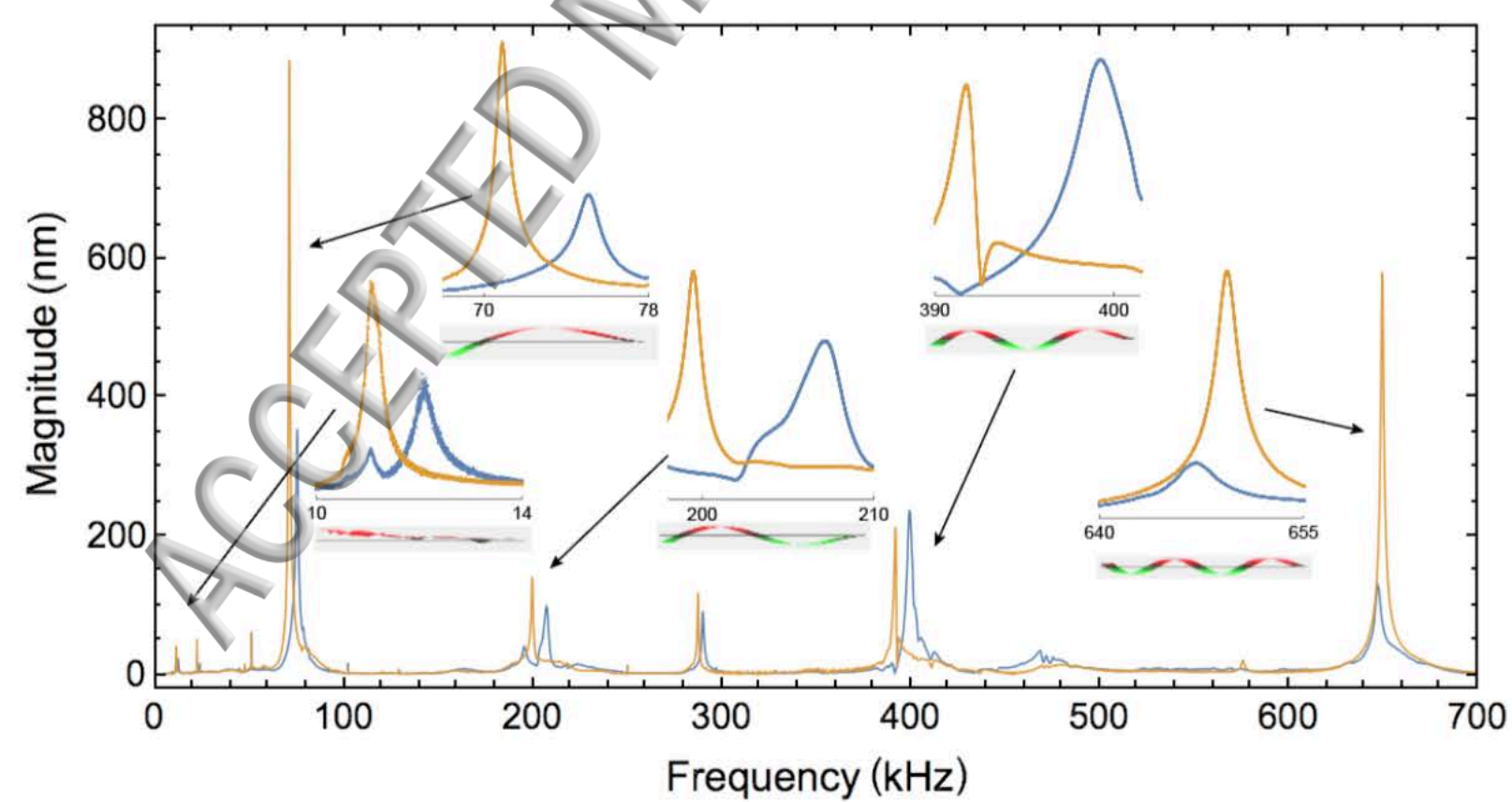
- <sup>1</sup>S. E. Cross, Y. S. Jin, J. Rao, and J. K. Gimzewski, *Nature Nanotechnology* **2**, 780 (2007).
- <sup>2</sup>S. E. Cross, Y.-S. Jin, J. Tondre, R. Wong, J. Rao, and J. K. Gimzewski, *Nanotechnology* **19**, 384003 (2008).
- <sup>3</sup>M. Plodinec, M. Loparic, C. A. Monnier, E. C. Obermann, R. Zanetti-Dallenbach, P. Oertle, J. T. Hyotyla, U. Aebi, M. Bentires-Alj, R. Y. Lim, *et al.*, *Nature nanotechnology* **7**, 757 (2012).
- <sup>4</sup>O. Malvar, J. J. Ruz, P. M. Kosaka, C. M. Domínguez, E. Gil-Santos, M. Calleja, and J. Tamayo, *Nature Communications* **7** (2016), 10.1038/ncomms13452.
- <sup>5</sup>J. J. Ruz, J. Tamayo, V. Pini, P. M. Kosaka, and M. Calleja, *Scientific Reports* **4** (2014), 10.1038/srep06051.
- <sup>6</sup>D. Martínez-Martín, G. Fläschner, B. Gaub, S. Martin, R. Newton, C. Beerli, J. Mercer,

- <sup>6</sup>C. Gerber, and D. J. Müller, *Nature* **550**, 500 (2017).
- <sup>7</sup>D. Ramos, J. Tamayo, J. Mertens, M. Calleja, and A. Zaballos, *Journal of Applied Physics* **100**, 2004 (2006).
- <sup>8</sup>D. Ramos, J. Tamayo, J. Mertens, M. Calleja, L. G. Villanueva, and A. Zaballos, *Nanotechnology* **19** (2008).
- <sup>9</sup>M. Calleja, P. M. Kosaka, Á. San Paulo, and J. Tamayo, *Nanoscale* **4**, 4925 (2012).
- <sup>10</sup>M. K. Ghatkesar, V. Barwich, T. Braun, J.-P. Ramseyer, C. Gerber, M. Hegner, H. P. Lang, U. Drechsler, and M. Despont, *Nanotechnology* **18**, 445502 (2007).
- <sup>11</sup>M. K. Ghatkesar, H.-P. Lang, C. Gerber, M. Hegner, and T. Braun, *PloS one* **3**, e3610 (2008).
- <sup>12</sup>Y. Zhang, *Sensors and Actuators, B: Chemical* **202**, 286 (2014).
- <sup>13</sup>E. Gil-Santos, D. Ramos, J. Martínez, M. Fernández-Regúlez, R. García, A. San Paulo, M. Calleja, and J. Tamayo, *Nature nanotechnology* **5**, 641 (2010).
- <sup>14</sup>R. R. Grüter, Z. Khan, R. Paxman, J. W. Ndieyira, B. Dueck, B. A. Bircher, J. L. Yang, U. Drechsler, M. Despont, R. A. McKendry, and B. W. Hoogenboom, *Applied Physics Letters* **96** (2010), 10.1063/1.3285169.
- <sup>15</sup>C. Liberale, G. Cojoc, P. Candeloro, G. Das, F. Gentile, F. D. Angelis, and E. D. Fabrizio, *IEEE Photonics Technology Letters* **22**, 474 (2010).
- <sup>16</sup>A. Zakhurdaeva, P. I. Dietrich, H. Hölscher, C. Koos, J. G. Korvink, and S. Sharma, *Micromachines* **8** (2017).
- <sup>17</sup>G. Göring, P. I. Dietrich, M. Blaicher, S. Sharma, J. G. Korvink, T. Schimmel, C. Koos, and H. Hölscher, *Applied Physics Letters* **109** (2016).
- <sup>18</sup>E. D. Lemma, F. Rizzi, T. Dattoma, B. Spagnolo, L. Sileo, A. Quattieri, M. De Vittorio, and F. Pisanello, *IEEE Transactions on Nanotechnology* **16**, 23 (2017).
- <sup>19</sup>A. A. Bauhofer, S. Krödel, J. Rys, O. R. Bilal, A. Constantinescu, and C. Daraio, *Advanced Materials* **29** (2017).
- <sup>20</sup>S. Maruo, O. Nakamura, and S. Kawata, *Optics Letters* **22**, 132 (1997).
- <sup>21</sup>S. Rast, C. Wattering, U. Gysin, and E. Meyer, *Review of Scientific Instruments* **71**, 2772 (2000).
- <sup>22</sup>Tamayo, Javier and Ramos, Daniel and Mertens, Johan and Calleja, Montserrat, *Applied Physics Letters* **89**, 1 (2006).
- <sup>23</sup>D. Ramos, M. Calleja, J. Mertens, Á. Zaballos, and J. Tamayo, *Sensors* **7**, 1834 (2007).

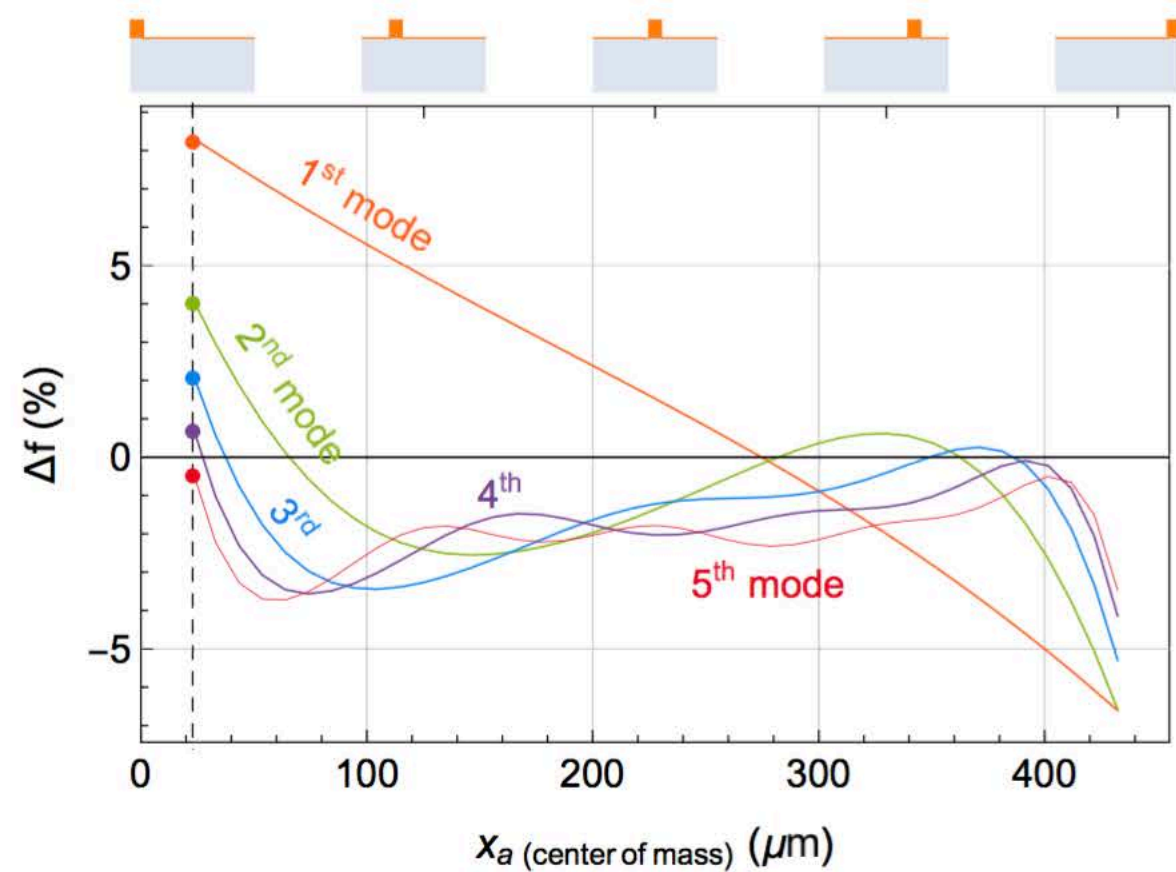
- <sup>24</sup>M. Amabili, S. Carra, L. Collini, R. Garziera, and A. Panno, *Journal of Sound and Vibration* **329**, 2057 (2010).
- <sup>25</sup>Rull Trinidad, E. and Gribnau, T. W. and Belardinelli, P. and Stauffer, U. and Alijani, F., *Applied Physics Letters* **111**, 123105 (2017).
- <sup>26</sup>G. N. Greaves, A. L. Greer, R. S. Lakes, and T. Rouxel, *Nature Materials* **10**, 823 EP (2011).
- <sup>27</sup>R. S. Lakes and A. Wineman, *Journal of Elasticity* **85**, 45 (2006).
- <sup>28</sup>H. Lu, X. Zhang, and W. G. Knauss, *Polymer Engineering & Science* **37**, 1053 (1997).

ACCEPTED MANUSCRIPT



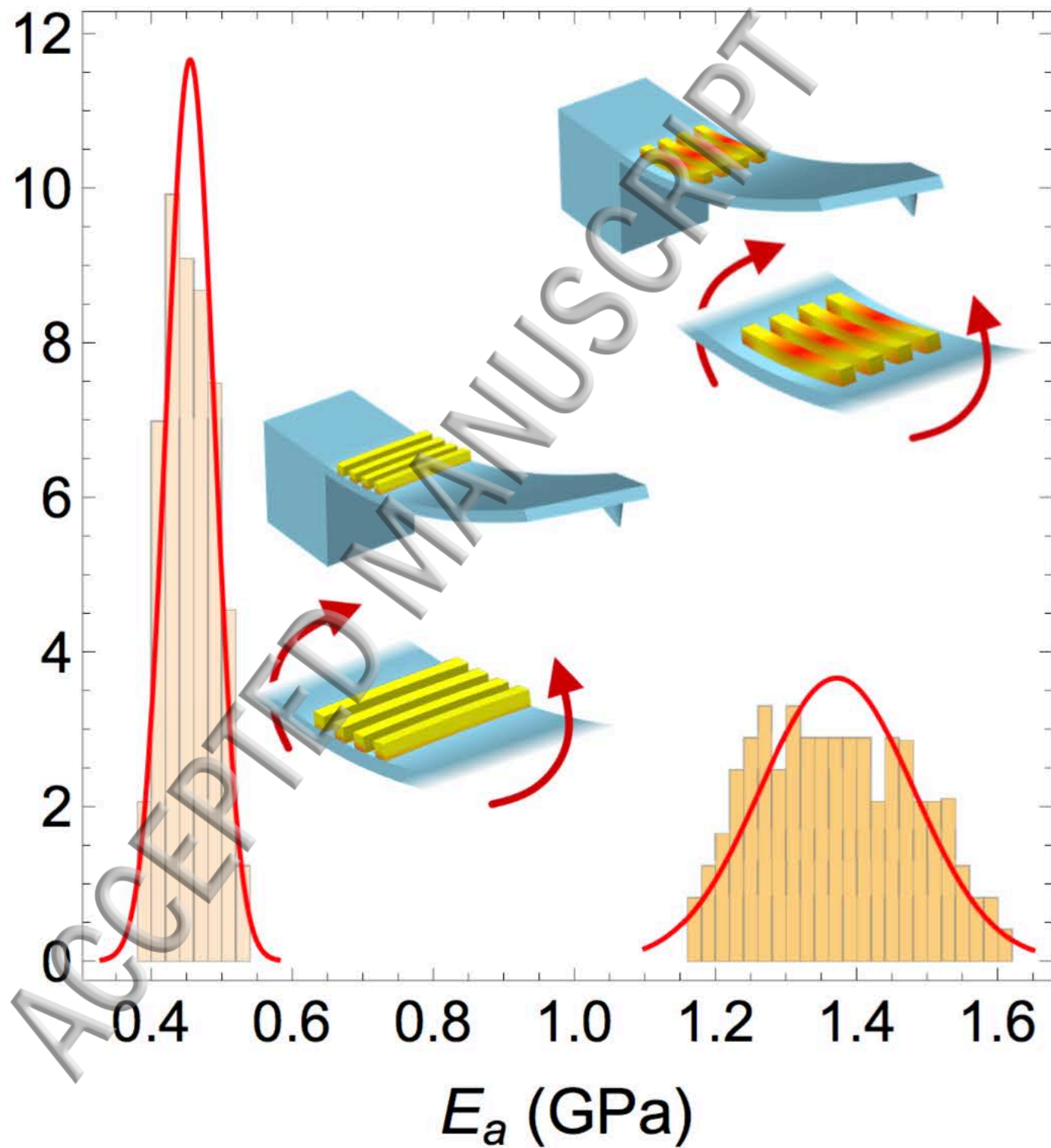


(a)

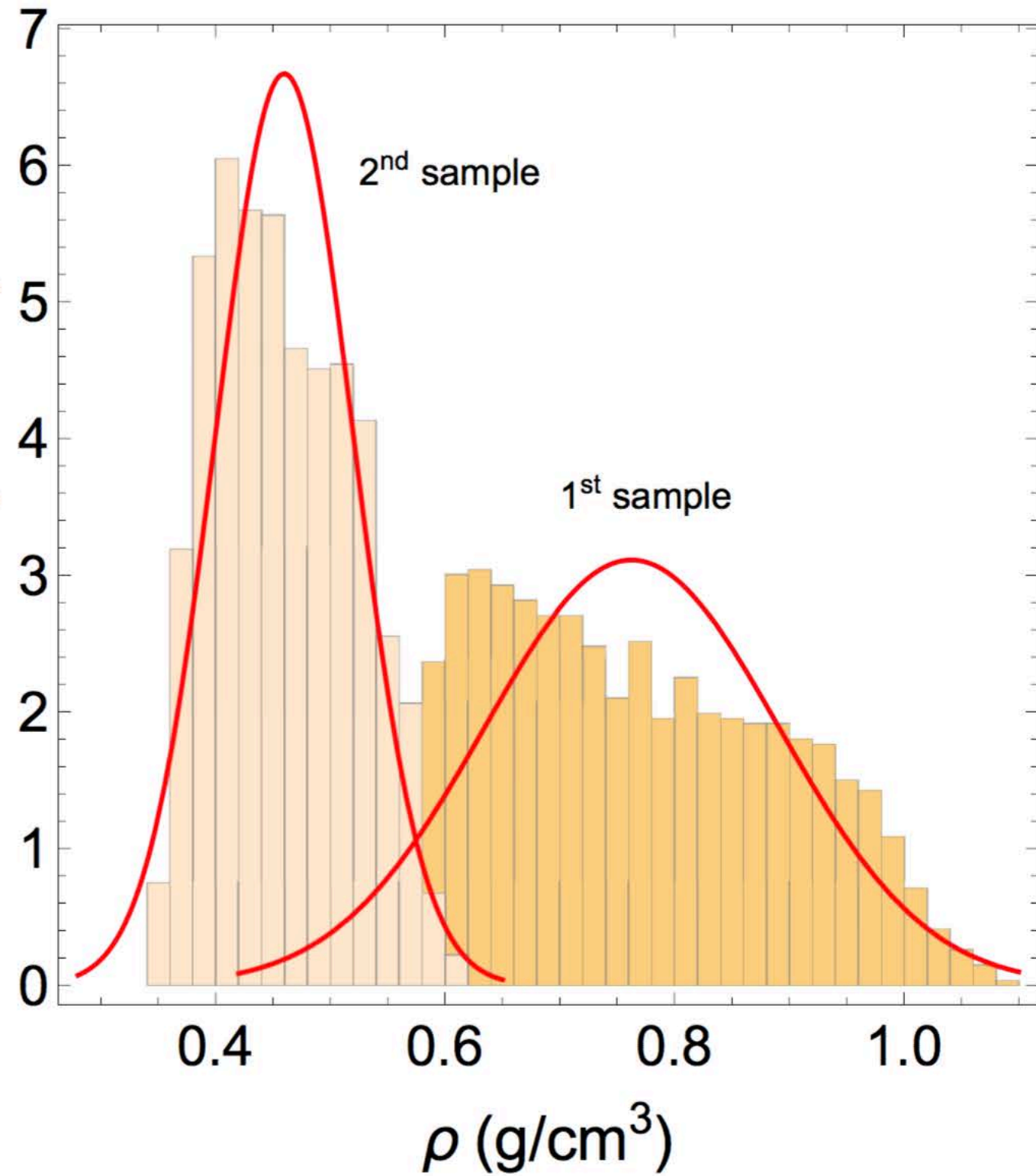


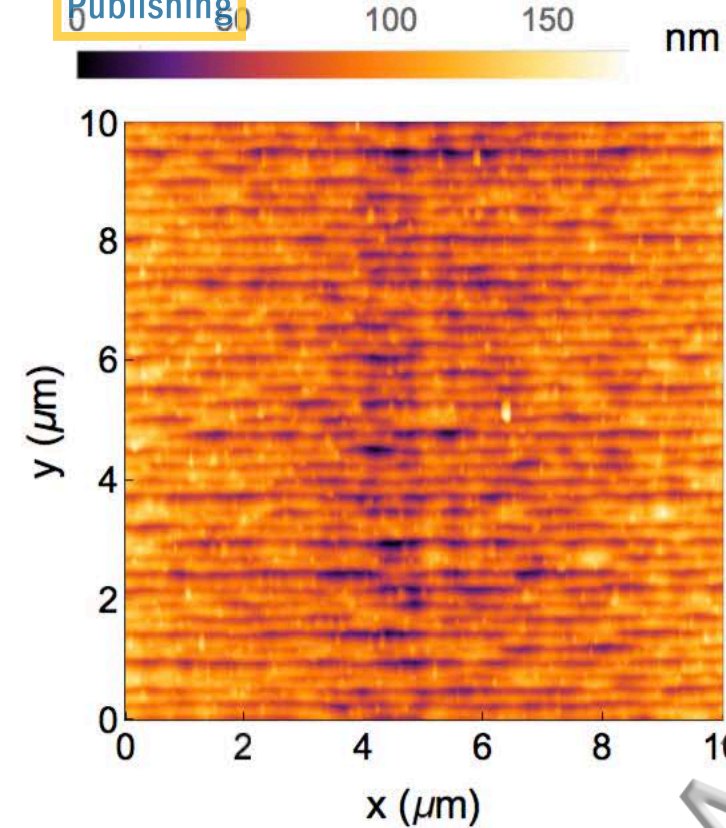
(b)

Probability density

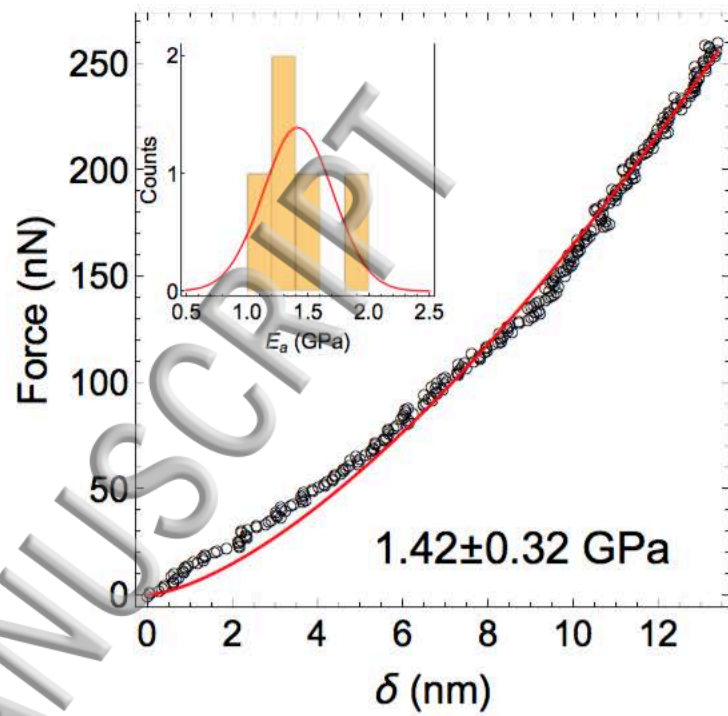


Probability density

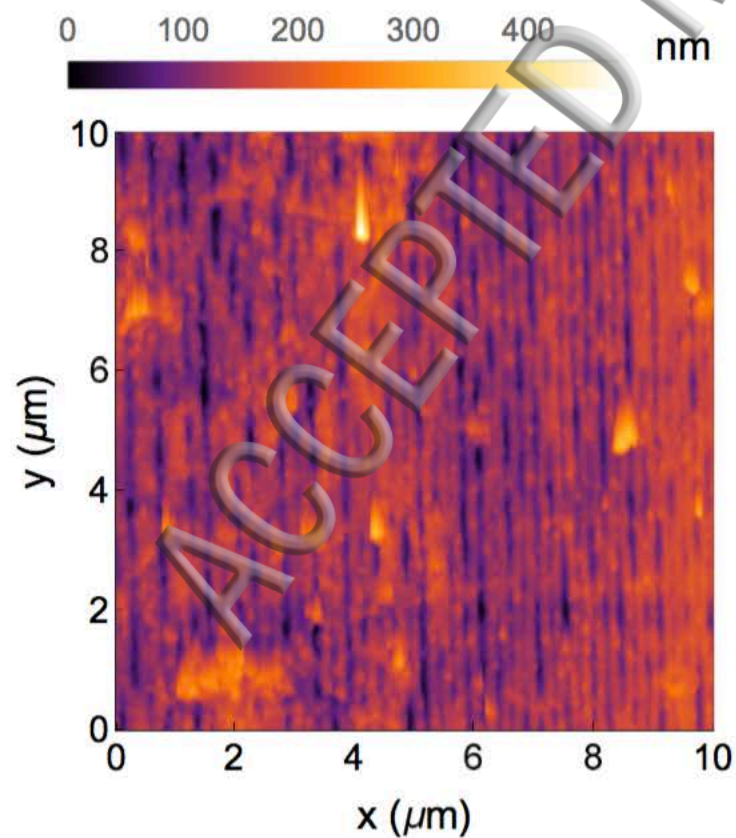




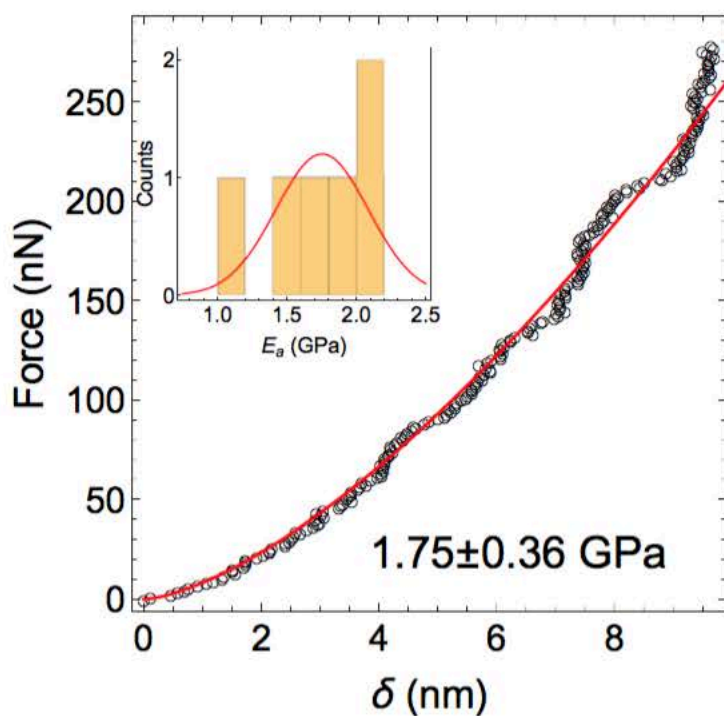
(a)



(b)



(c)



(d)